

ACCELERATED STRESS TESTING OF TERRESTRIAL SOLAR CELLS*

J. L. Prince, J. W. Lathrop, and F. W. Morgan
Clemson University
Clemson, SC 29631

E. L. Royal
JPL
Pasadena, CA 91103

G. W. Witter
OCLI
City of Industry, CA 91746

Abstract

The results of a program to investigate the reliability characteristics of unencapsulated low-cost terrestrial solar cells using accelerated stress testing are presented. Four types of cells were investigated. Reliability (or parametric degradation) factors appropriate to the cell technologies and use conditions were studied and a schedule of accelerated stress tests was synthesized. An electrical measurement procedure capable of distinguishing small changes in cell electrical parameters was established. A data analysis and management system was derived, and stress test fixturing and material flow procedures were set up after consideration was given to the number of cells to be stress tested and measured and the nature of the information to be obtained from the process. Based on both electrical parameters and metalization adherence strength, significant degradation was shown by some cell types in some stress tests. Other combinations of cell types and stress tests resulted in no detectable cell degradation. Analysis of the origins of the differences in degradation is continuing.

Introduction

The reliability characteristics of solar cells intended for terrestrial applications will be a key factor in determining whether the national goals for solar photovoltaic power generation can be met in a timely fashion. DoE cost goals set for terrestrial cells have been based on the assumption of a 20-year module life; however, no data have existed in the past to support this reliability assumption for appropriate cell technologies and environmental conditions. Very little is found in the open literature concerning the nature of the time-to-failure (TTF) distributions of solar cells in terrestrial ambient conditions, the failure modes and failure mechanisms which control the TTF distributions, the appropriate methods for accelerated stress testing for reliability verification, or the process modifications required to upgrade reliability performance. In fact, the status of the subject is such that viable failure criteria do not exist. Depending on the parameter involved, and within certain limits, changes in cell parameters may well simply result in changes in efficiency of power generation of a photovoltaic system. Firm definition of cell interconnection

techniques within system subassemblies and configuration of subassemblies to form systems, and classification of system applications, would aid in defining degradation limits for failure. Such a definition does not currently exist. Thus variables data are needed in addressing the subject. Also, the concepts of failure and failure rate should be replaced by degradation and degradation rate.

The program which led to the results reported here represented the first systematic attempt to define the reliability attributes of terrestrial solar cells. Goals of the program were not only to establish a base line for the reliability of present, commercially available, state-of-the-art cells, but also to develop methodology which would permit the intercomparison of cells and manufacturing technologies both now and in the future. Quantification of reliability is not a simple matter, particularly for cases where no prior data exist. Experience in the field must be the ultimate verification of a device's reliability, but for a number of reasons, it is often not practical to attempt to define reliability from field test data: the times are so great to obtain significant numbers of failures, that the technology will have completely changed by the time reliability data are in; or the numbers of devices required on test is prohibitively large; or lack of experimental controls results in erroneous results. In the case at hand, field degradation data for cells are practically nonexistent. Also, reliability expectations for cells, and field deployment plans, are such that many systems may be in operation before sufficient field data are generated to make reliability (or degradation rate) estimates. Thus the approach taken here, that of projecting solar cell degradation modes and mechanisms, choosing accelerated stress tests in the light of this projection and in light of field conditions, and applying the stress tests to sensible quantities of commercially available cells, represents the only viable approach to solar cell reliability assurance at this point.

Solar Cell Physical Characteristics

Four cell types from four different manufacturers were available for stress testing. These were state-of-the-art conventional terrestrial cells fabricated from Czochralski-grown single crystal silicon substrates. All cells had one or more tabs attached by the

*This paper presents results of research performed for the Low-Cost Solar Array Project, Jet Propulsion Laboratory, California Institute of Technology, sponsored by the U.S. Department of Energy through an interagency agreement with NASA.

manufacturer to the top surface, but were only metalized on the back side. The tab material and tab attachment method was identical to each manufacturer's practice for cells used in terrestrial arrays. Table 1 summarizes the physical characteristics of the stress test cell types.

Table 1. Physical Characteristics of Stress Test Cells

PHYSICAL CHARACTERISTICS OF CELLS

TYPE	DIAMETER (in)	THICKNESS (mils)	A R COATING	TECHNOLOGY	METAL
A	4	24	NO	P/N	SOLDER
B	3	19	YES	N/P	THIN FILM Ti/Pd/Ag
C	2	20	YES	N/P	SOLDER
E	3	15	NO	N/P	THICK FILM Ag

Solar Cell Characterization

Two types of measurements were performed on stress test populations, electrical parameter determination and metal adhesion strength determination. Electrical measurements were made at a thermocouple monitored temperature of $28 \pm 0.5^\circ\text{C}$ under ELH lamp illumination of $100\text{mW}/\text{cm}^2$ irradiance, corresponding to 1-sun at air mass 1 (AM-1). For each of the four cell types a reference cell, calibrated by Jet Propulsion Laboratory under true sunlight conditions, was used to adjust the irradiance of the measurement system light source to its proper value. This reference cell was used to check the uniformity of the ELH simulator across the field of the cell and to insure the absence of lamp drift with time. A Kelvin probe, vacuum hold down, water cooled jig was used to contact the cells. The 4-point Kelvin probe connections eliminated spurious resistive effects and assured repeatable readings. Parameters measured were the short-circuit current and open-circuit voltage, I_{sc} and V_{oc} , and the illuminated fourth-quadrant cell I-V characteristic. From these the maximum cell power output, P_m , and the cell output voltage and current at the maximum power point, V_m and I_m , were determined. The illuminated far-forward diode characteristic was also obtained. Figure 1 shows the V-I characteristics of a cell illustrating the measurement repeatability obtained over an extended period (4 months) for each of these parameters. Measurements were performed before the application of stress and at periodic down-times during the stress test.

Metal adhesion strength was measured (destructively) using a Unitek Micropull Strength Tester with a Chatillion Force Gage. Adhesion strength was measured on a random sample of 25 unstressed cells per cell type, and on a small sample of stressed cells of each type from each stress test at one point during the

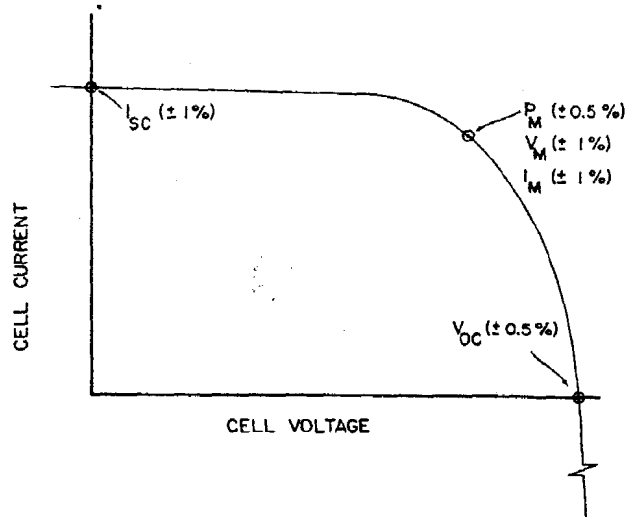


Figure 1. Cell I-V Characteristic, with Electrical Parameters

testing. Both manufacturer's attached tabs and solder-attached test leads were used in the metal adherence strength measurements.

In the stress test program each cell was assigned a serial number, photographed using high resolution film, and stored in a plastic petri dish. In all, approximately 400 cells of each type were serialized and photographed. Electrical parameters were measured and the cells visually inspected under 7-10X magnification. The electrical measurement and visual inspection were performed at each subsequent test down-time; however, cells were photographed at down-times only when highly physical effects were found under visual inspection. Before being stressed and at down-times the cells were normally stored either under dry nitrogen or in a low-humidity laminar flow hood. Cells were not cleaned before insertion into the stress testing flow even though some clearly were dirty as received from the manufacturers. It was felt that cleaning might introduce anomalies into the stress test results. In addition, no further cleaning would normally be performed on the cells, prior to assembly into modules, by the manufacturer.

Accelerated Stress Test Program Development

Potential Failure Mechanisms

Likely failure mechanisms of terrestrial solar cells were projected after consideration of state-of-the-art conventional cell technology, use conditions, and the body of physics of failure information obtained from semiconductor devices. "Failure mechanisms" as used above may be a misnomer; "degradation mechanisms" may be the proper phrase for the case at hand. Since conventional cells are fabricated using single crystal silicon starting material, and since the only surface exposure of the junction occurs at the slice edge, enhanced impurity diffusion effects and many of the oxide and oxide-silicon interface effects which affect microelectronic devices were not expected to be a factor in

terrestrial solar cell parameter stability. However, several mechanisms exist which can affect the solar cell metalization system, particularly the front-side collector and grid metalization, under use conditions. The cell metalization system directly affects some cell electrical parameters such as P_m through series resistance R_s . Changes in the average resistivity of a front-side metal stripe due to corrosion, electromigration phenomena, or metal segregation phenomena in compound cell metalization systems, changes in the metal-silicon contact resistance due to interdiffusion or corrosion of contacting metal layers, or changes in interconnect-metal contact resistance due to electromigration or Kirkendall voiding, can result in degradation of P_m due to increase in R_s . Some of these can also decrease the metal adherence strength. Likewise, decrease in the cell shunt resistance due to metal plating from the front to the back of the cell at the cell perimeter or due to penetration of the cell junction by metal ("contact spiking" in integrated circuit jargon) can result in degradation of P_m . Delamination of metalization, or reduction in metal adherence strength due to thermally induced mechanical stresses, were also considered to be likely use condition phenomena. In addition to the degradation mechanisms considered to be likely in the field, connected with the metalization, it was also considered possible that cell cracking and antireflective (AR) coating cracking might occur under conditions of thermally induced mechanical stress, and that decomposition of the AR coating might occur under humidity-temperature stress.

After performing a more complete analysis using the sort of rationale shown above, the degradation mechanisms most likely to affect terrestrial cells, and which should be accelerated in a cell reliability investigation, were chosen. These degradation mechanisms, and their associated stresses, are shown below in Table 2. In this table B = electrical potential (bias), I = current, t = time, T = temperature, and H = humidity.

Table 2. Degradation Mechanisms Likely to Affect Terrestrial Solar Cells

Degradation Mechanism	Accelerating Stress
Corrosion	BTH
Kirkendall Voiding	T
Electromigration	I, T
Contact Spiking	I, T
Metal Segregation	T, dT/dt
Electroplating	BTH
Metal Delamination	dT/dt, BTH, T
Cell Fracture	dT/dt
AR Coating Fracture/ Delamination	dT/dt
AR Coating Decomposition	TH

Note that although light could be considered a stress, it was not included in the considerations due to the scope of the investigation. The facilities and fixturing problems entailed

in using light as a stress test condition are manifold.

Test Schedule

Based on the projected failure mechanisms, and on existing stress tests such as are contained in Military Method MIL-M-38510 and Military Standard MIL-STD-883A, a repertoire of stress tests for terrestrial solar cells was selected. From this point, the approach to determining the final stress test schedule including population size, times, and exact test conditions was two-fold. First, the problem was scoped using simplistic methods. Practical limits to stress testing conditions, such as the melting at 170°C of the solder used for metalization and lead attachment, were determined, and certain gross assumptions concerning acceleration factors, and use-condition degradation rates, were made where possible. An example of an assumption made strictly to obtain general information on times involved was the assumption that under bias and temperature stress only, degradation mechanisms would proceed according to an Arrhenius relationship with an activation energy of 1 eV. A tentative stress test design was performed under these limits and assumptions, keeping in mind the need for test populations large enough to identify infant mortalities as such. Needless to say, constraints of time and money played a part in the selection of the stress test schedule. Then, after selection of the stress tests, small quantities of units (e.g., five units per cell type) were subjected to abbreviated tests in order to determine the magnitudes of change in electrical parameters, and the time rate of the change, which could be expected from the full-scale tests. The nature and degree of physically observable effects to be expected in the large scale tests was also determined in the small scale experiments. Results from these experiments were used to choose initial down-times for the large-scale tests. Subsequent down-times in the large-scale tests were chosen depending on effects observed at earlier down-times, and depending on electrical measurement scheduling and capacity.

Table 3 shows the resultant large-quantity stress test schedule. For most tests there were either three or four down-times. Contact integrity measurement was performed only at the first down-time, and units subjected to this (destructive) test were removed from the test population. All stress tests performed using bias utilized diode forward bias. This is the proper polarity potential, compared to the polarity in field use, for corrosion and electroplating degradation mechanisms. However, the direction of current flow is opposite to that which exists under active, generating conditions. Since light was not used in the stress testing, the compromise of forward current direction as opposed to reverse direction was necessary. The BT tests utilized forward bias currents of from 1.2A to 3.3A, approximately scaled by the cell short circuit current and area, while the BTH tests used forward bias voltages of approximately 0.45V. At 85°C, the diode forward current for 0.45V forward voltage varied from

Table 3. Stress Test Schedule

STRESS TEST SCHEDULE		
STRESS TEST	TEST POPULATION PER CELL TYPE	STRESS TEST DURATION
BIAS-TEMPERATURE, 75°C	50	2800 hr
BIAS-TEMPERATURE, 135°C	50	2300 hr
BIAS-TEMPERATURE, 150°C	40	1400 hr
BIAS-TEMPERATURE, 165°C	40	1200 hr
BIAS-TEMPERATURE-HUMIDITY, 121°C/15 Psig	20	300 hr
BIAS-TEMPERATURE-HUMIDITY, 85°C/85% R.H.	25	1000 hr
POWER CYCLE	25	25K CYCLES
THERMAL CYCLE	20	65 CYCLES
THERMAL SHOCK	15	35 CYCLES

0.3A to 1A, depending on cell type. In the Power Cycle Tests the cells were forward biased ($I_F = 1.5$ to 3.6A, depending on the cell type) for two minutes and turned off for two minutes.

Discussion and Results

Results of this study fall into two primary categories, electrical parameter degradation and contact integrity degradation versus stress. The key cell electrical parameter is P_m , which is affected by I_{sc} and V_{oc} and which can also be strongly influenced by R_s and R_{sh} . Thus the electrical impact of the stress tests can be expressed in terms of the effect on P_m . The results are organized such that electrical parameter effects, and in some cases visually evident effects, are grouped according to stress test categories, while the contact integrity effects due to all stress tests are discussed together.

BT Stress Test Results

Figures 2 and 3 show examples of the observed effects of BT stress on P_m for all types. In these figures the mean percent decrease of P_m for the four cell types, calculated on a cell-by-cell basis, is shown versus stress time for two of the BT stress tests. From results shown in these figures it is clear that no degradation in P_m was experienced by type B cells, and that relatively severe and consistent degradation in P_m was experienced by type A cells. These conclusions are borne out by data from the other two BT stress tests. Figure 4 shows the response of type A cells at all four stress test temperatures. Less obvious is the response of the type C and E cells. For type C cells a generally monotonic (though small) decrease in P_m with stress time was observed for the higher two stress temperatures; however, the results from the two lower temperature tests showed no discernable P_m degradation. It is

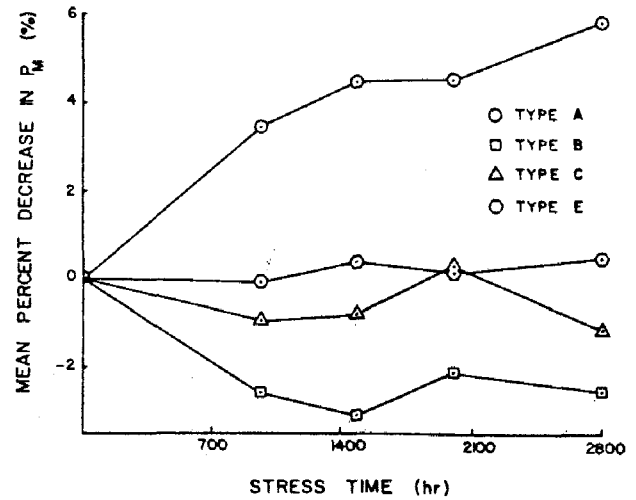


Figure 2. Mean Percent Decrease in P_m for 75°C Bias-Temperature Stress Test, All Cell Types.

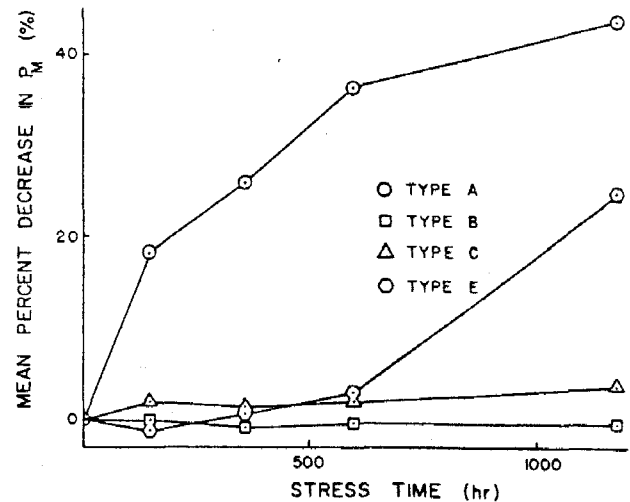


Figure 3. Mean Percent Decrease in P_m for 165°C Bias-Temperature Stress Test, All Cell Types.

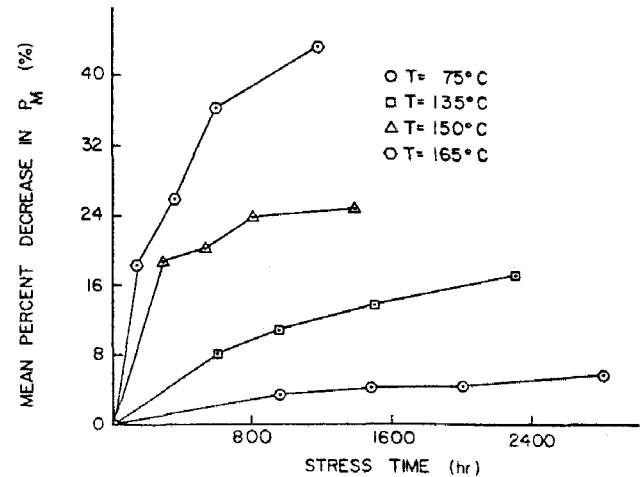


Figure 4. Mean Percent Decrease in P_m , Type A Cells, Bias-Temperature Stress.

clear that additional data are required before the question of degradation, and degradation rate, can be resolved for this cell type. For type E cells it is somewhat clearer that degradation occurred in bias-temperature testing. However, the amount of degradation was smaller than that shown by the type A cells and again was evident only in the two higher temperature stress tests. Interpretation of the data for type E cells is made difficult by the large incremental degradation shown at the last down-time in Figure 3. Thus additional data are also required for this cell type before degradation, and degradation rate, can be quantified.

For the type A cells, analysis of I-V far-forward data showed that the observed degradation in P_m was due at least partially to an increase in R_s . As an example of the influence of increasing R_s on the cell I-V characteristics, Figure 5 shows I-V data for a typical cell subjected to the 165°C bias-temperature stress. The effect of the increase in R_s with increasing stress test time is evident to the right of the knee of the curves in this figure.

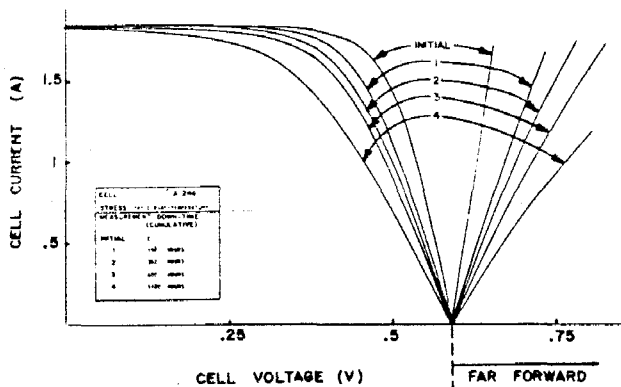


Figure 5. Type A Cell I-V Characteristics After 165°C B-T Stress, Typical Case.

Figure 6 shows the behavior of R_s with bias-temperature stress time for a typical type A cell from each stress test lot. The values of R_s shown in this figure were obtained from the slope of the I-V characteristic in the neighborhood of the zero external cell current point. They were not obtained from the portion of the far-forward I-V characteristic which shows obvious downward concavity. Although increase in R_s certainly accounts in large part for the observed decrease in P_m for these cells, the specific mechanism responsible for the increase has not been identified. However, it was noted that relatively large (1-2 mm), hollow bubbles appeared in the collector and grid solder during the stress tests. These bubbles occurred least frequently (approximately 30% of the stress test population) in the 75°C stress test and most frequently in the 165°C stress test, and increased in size and frequency of occurrence with increasing stress time. No correlation

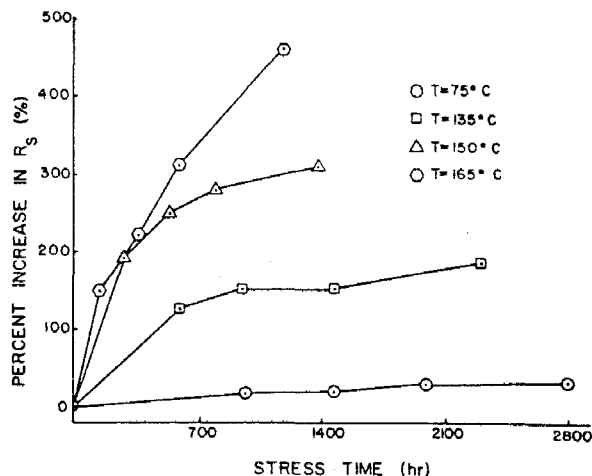


Figure 6. Behavior of R_s with B-T Stress Time, Typical Type A Cells.

between bubble occurrence and P_m degradation on a cell-by-cell basis has been performed to date. Type C cells, which also had solder as the primary component in the metalization system, exhibited collector and grid bubbles much less frequently than did the type A cells, and the degree of degradation of P_m was much less severe for type C cells.

From earlier discussion it is clear that projections to use conditions of the degradation rate due strictly to bias and temperature are not warranted by the data for three cell types. In fact, the type B cells investigated did not degrade under this stress to any detectable degree. However, data for type A cells do permit a crude extrapolation of the degradation rate to use conditions. In order to do this it is necessary to somehow extrapolate (or interpolate) the P_m degradation data for the various tests to a common degradation level. It was noted, for the type A cells, that a plot of the cumulative mean percent P_m degradation versus time on lognormal paper resulted in acceptably straight lines for three stress test temperatures, 75°C, 135°C, and 165°C. Other types of plots of the raw data were made and in every case the 150°C data did not fit the pattern exhibited by the data from the other three tests. The 150°C stress test data was thus ignored in subsequent analyses. Figure 7 shows the behavior of the time to 10% P_m degradation versus inverse absolute stress test temperature, for type A cells. In this figure are shown two straight line fits to the three data points. Line A was obtained ignoring the 165°C stress test data altogether, and is attributable to a mechanism having an activation energy of slightly greater than 0.4 eV. Line B was obtained taking into account all three data points, and is describable by a mechanism having an activation energy in the neighborhood of 0.6 eV. Extrapolation of the two lines to 50°C results in a range of 2×10^4 hr to 7×10^4 (2 to 10 years) as an estimate of the time to 10% degradation for type A cells at that temperature.

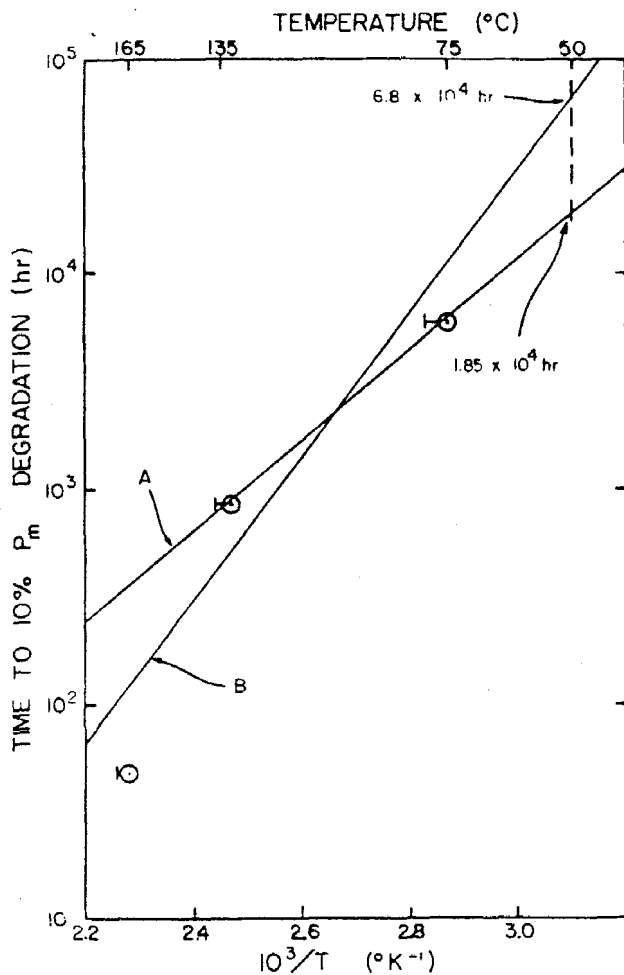


Figure 7. Behavior of Time to 10% Degradation Versus Inverse Temperature, Type A Bias-Temperature Stress Test Lots.

Although the analysis above was done in order to obtain some information on use-condition degradation rates due strictly to current and temperature for type A cells, the data clearly do not permit a precise prediction of the field degradation rate. Far more data will be required on all cell types before definite "life" prediction can be made. What the data absolutely do show is that type A cells do exhibit definite P_m degradation under the stress test conditions even at relatively low temperatures, and that this degradation is associated with an increase in R_s .

BTH Stress Test Results

Figures 8 and 9 show observed mean percent decrease in P_m versus test time for the biased 85°C/85% R.H. and biased 121°C/15 Psig steam stress tests respectively. From data presented in these figures it is clear that type B cells showed the least degradation in P_m under both types of B-T-H stress testing (approximately zero effect for 85/85 stress and only minor effect for pressure cooker stress) and that type E cells showed

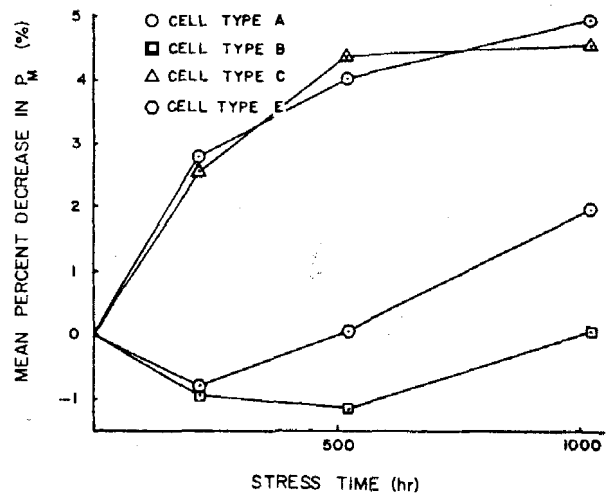


Figure 8. Mean Percent Decrease in P_m versus Stress Time, Biased 85°C/85% R.H. Test.

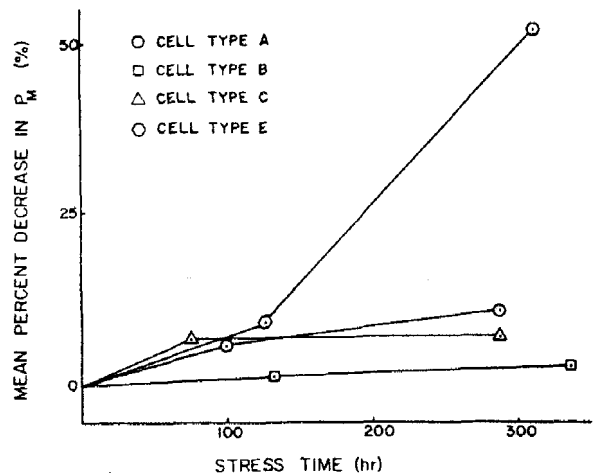


Figure 9. Mean Percent Decrease in P_m versus Stress Time, Biased 121°C/15 Psig Steam Test.

relatively severe P_m degradation in the pressure cooker stress test. The source of this difference in response of type E cells is not clear. Distortion of the I-V plot was so severe for the pressure cooker-stressed type E cells at the second down-time that straightforward interpretation of the results to determine the source of the degradation was not possible. By analogy to the I-V plots of the type A cells which showed similarly severe P_m degradation under B-T stress, due to R_s increase, it would appear that R_{sh} of the type E cells decreased thereby causing the decrease in P_m . However, firm conclusions in this regard must be delayed until further analysis is performed.

Type A and type C cells showed definite, but less severe P_m degradation in the pressure cooker stress test. The P_m degradation for these two types was more severe than for the type E cells in the 85/85 test. For type C cells the source of the P_m degradation in both stress test lots can be traced to decrease in I_{sc} due to degradation of the AR coating. Table 4 shows the mean percent decrease in P_m and in I_{sc} for the two type C B-T-H test lots.

Table 4. Mean Percent Decrease in P_m and I_{sc} , versus BTH Stress Test Time, Type C Cells.

	85°C/85% R.H.			121°C/15 Psig	
	215 hr	525 hr	1025 hr	76 hr	286 hr
MEAN PERCENT DECREASE IN P_m (%)	2.55	4.35	4.55	7.02	7.37
MEAN PERCENT DECREASE IN I_{sc} (%)	2.74	3.59	3.57	6.19	6.62

The correlation in degradation of the two parameters is obvious, and the nature of the degradation correlates with the physical appearance of the cells after stress testing. The source of the decrease in P_m of the type A cells has not yet been identified positively, but is probably an increase in series resistance similar to that which was discussed earlier for type A cells subjected to BT stress testing. This is plausible since the temperatures involved were similar, the degree of degradation in P_m was similar, and solder bubbles were manifested in both B-T and pressure cooker stress tested units. Thus the degradation in P_m for type A cells resulting from BTH stress may well be due strictly to temperature effects, and possibly bias effects, and not due to humidity stress.

It did not appear to be appropriate to extrapolate the results obtained to use conditions due to the small number of BTH stress levels employed in the program. Although significant work on BTH acceleration factors has been done for integrated circuits, it is not clear based on work to date what degradation mechanisms are active for solar cells, and the applicability of previously derived factors is thus not established. Further work must be done in this area.

Thermal Cycle/Shock Stress Test Results

Based on results of small-quantity experiments the thermal cycle step-stress schedule shown on Table 5 was used in the large-quantity stress testing. The initial test population was 20 cells per type. Eight cells per type were removed for contact integrity measurement after the third down-time. The physical effects observed in thermally

Table 5. Thermal Cycle Stress Test Schedule.

STRESS LEVEL / DOWN-TIME NUMBER	NUMBER OF CYCLES	ELECTRICAL MEASUREMENT
0°C TO +150°C/(1)	10	YES
+		
-25°C TO +150°C/(2)	10	YES
+		
-45°C TO +150°C/(3)	10	NO
+		
-65°C TO +150°C/(4)	10	YES
+		
-65°C TO +150°C/(5)	10	NO
+		
-65°C TO +150°C/(6)	15	YES

cycled units generally fell into one or more of three categories: type X breaks (conchoidal silicon fractures normally located under the tab attachment points); type Y breaks (regions of delaminated metal on either the cell front or back); and type Z breaks (long silicon fractures apparently along preferred breakage planes usually initiated or terminated in the vicinity of the tab attachment points). Figures 10 through 12 show examples of these three types of effects. Tables 6 and 7 show physical effects observed for two of the cell types. The data shown in Table 7 are complete; no breaks other than type X breaks were observed. The type C cells showed a response different from that shown in these tables. For this cell type, delamination of back-surface metalization was noted beginning at down-time number 3; eventually seven of the twelve units showed this effect. The response of type E cells was similar to that of the type A cells except that metal delamination did not occur. The effects of thermal shock stress were similar to those observed for thermal cycle stress. The effects of thermal shock were no more severe than those of thermal cycling; in fact, if anything they were less severe.

Relatively minor electrical effects were found poststress for both thermal cycle and thermal shock stress. This was in spite of the fact that in many cases the tabs were held in place after stress only by the tensile strength of the thin metal layer, and in some cases the cell itself was held together solely by portions of the metalization which functioned as "tape." However, the cells were in a relatively aseptic environment during the thermal cycling and electrical measurement operations; the field environment of a module would be quite different and electrical effects of the various "breaks" may show up in

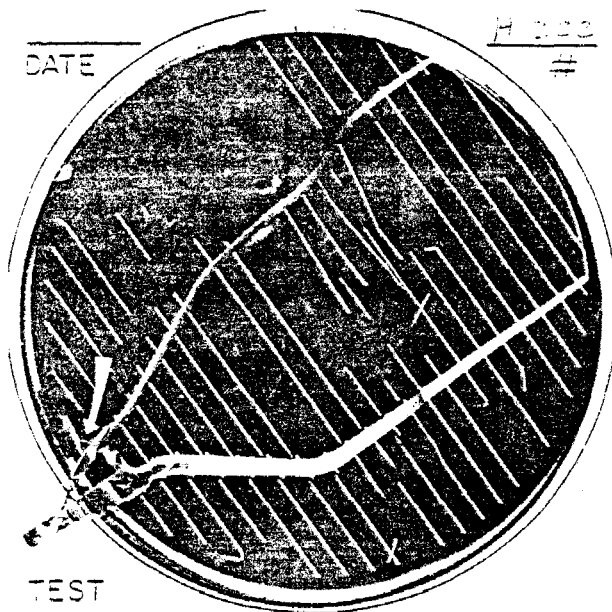


Figure 10. Type A Cell with Collector and Grid Delamination (Type Y Break) and Type X Break (Arrow).

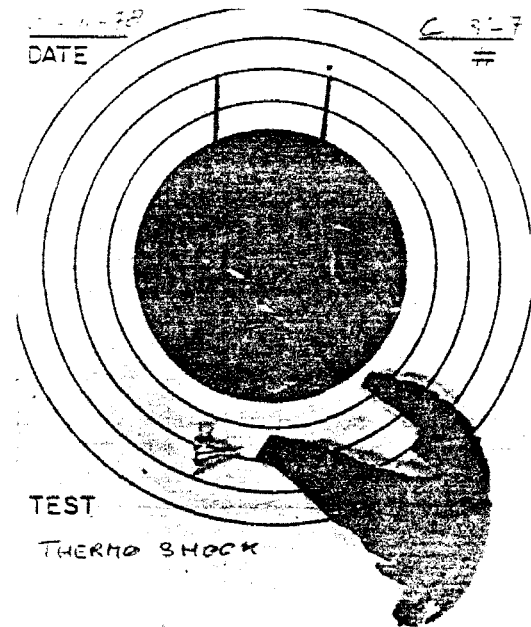


Figure 11. Type C Cell with Delamination of Back Metal (Type Y Break).

Table 6. Physical Effects Observed During Thermal Cycle Stress Testing, Type A Cells.

DOWN-TIME NUMBER	CELLS IN TEST	CELLS EXHIBITING TYPE X BREAKS (CUMULATIVE)	CELLS EXHIBITING TYPE Y BREAKS (CUMULATIVE)	CELLS EXHIBITING TYPE Z BREAKS (CUMULATIVE)
1	12	0	0	0
2	11*	5	0	0
3	11	9	5	0
4	11	10	5	1
5	8	10	9	1
6	8	10	10	2

*ONE CELL REMOVED DUE TO ACCIDENTAL BREAKAGE

Table 7. Physical Effects Observed During Thermal Cycle Stress Testing, Type B Cells.

DOWN-TIME NUMBER	CELLS IN TEST	CELLS EXHIBITING TYPE X BREAKS (CUMULATIVE)
1	12	0
2	11*	2
3	11	6
4	11	6
5	11	6
6	11	6

*ONE CELL REMOVED DUE TO ACCIDENTAL BREAKAGE

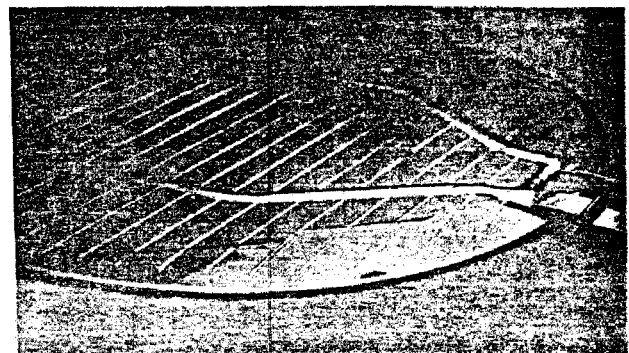


Figure 12. Type A Cell with Long Silicon Fracture (Type Z Break).

real time. The insensitivity of P_m to this type of stress, under laboratory conditions, illustrates the importance of visual inspection as a part of the characterization procedure.

From the foregoing information it is clear that the tab attachment area is a likely failure point under thermo-mechanical stress for all but type C cells. This is true even for type B and E cells, which had very small amounts of solder used in the tab attachment operation. Strangely, the worst-performing cell under thermal cycle stress was the heavily solder-metalized type A cell, and the best-performing cell was the heavily solder-metalized type C cell. Without details of the substrate silicon characteristics and the lead attachment process it is not possible to determine the source of this performance difference, although several possibilities exist including simply the cell size.

Power Cycle Stress Testing

Essentially no electrical effects of power cycle stress were observed. For example, at the final down-time (25,000 cycles) it was found that P_m had decreased approximately 2% for cell types A and E, and increased approximately 2% for cell types B and C. Clearly none of the cell types were electrically sensitive to repeated shallow (5°-10°C) thermal cycles.

Stress Test Effects on Contact Integrity

Results of measurement of the contact integrity of stress tested solar cells are given in Table 8. The data of this table were obtained by destructively pulling the tab attached by the cell manufacturer. Similar

Table 8. Contact Integrity Effects of Stress Tests

CONTACT INTEGRITY TEST RESULTS

STRESS TEST	RELATIVE METAL ADHERENCE STRENGTH			
	TYPE A	TYPE B	TYPE C	TYPE E
BIAS-TEMPERATURE	0.4-0.6	0.5-1.2	0.6-0.7	0.7-1.0
PRESSURE COOKER	0.6	1.3	0.35	1.1
85°C/85% R.H.	0.9	1.4	1.0	1.3
POWER CYCLE	1.0	1.0	0.8	1.0
CONTROLS	1.0			

results were obtained by destructively pulling 2mm wide Cu ribbon soldered to the cell after stress testing. Attempts to use 2mm wide Cu ribbon attached by epoxy as a test lead were not successful. The cells used in the contact integrity measurements were removed from the stress test lots at the first down-time except for the thermal cycle stress test units.

These units were removed after the third 10-cycle step of the step stress schedule. Quantities of units subjected to this measurement ranged between seven and ten units per cell type per stress test. In addition, 25 control units per type which had not been stress tested were used to set the base line for comparison of stress tested units.

Considering the data shown in Table 8 and other data obtained in the course of the measurements, it is clear that both BT and BTH pressure cooker stress generally had strong deleterious effects on contact adherence, and that power cycle stress had essentially no effect. Of particular interest is the degradation shown for the pressure cooker-stressed units, and the lack of degradation shown by the 85°C/85% R.H.-stressed cells for types A and C cells. This degradation (or lack thereof) was repeated in the measurements made using separate Cu ribbon test leads. The cause of the degradation in the one case, and lack of degradation in the other case, is under study.

Conclusions

The usefulness of an accelerated stress test program in discriminating between cell types and technologies has been demonstrated. This discrimination could be observed on the basis of P_m degradation, visual observation, and metalization adherence degradation. Accelerated testing of unencapsulated cells should be a useful technique of rank-ordering cell types with respect to their potential field reliability. When applied systematically to production run samples the method should be usable as a quality control monitor and should be a key element in identifying problems with reliability implications. Accelerated stress testing is a must for timely performance of these reliability assurance functions.

Figures 13 and 14 summarize the relative effects of the various stress tests on P_m and contact integrity for the four cell types investigated. In these figures, the darkest squares signify a degradation which was progressive with stress test duration, and significantly above the "noise" of the measurement technique. The lightest squares signify no discernable effect after stressing. "Medium" squares denote cases between the two extremes. Obviously subjective judgement was used in formulating the figures.

It can be seen from an examination of the columns in these figures that type A cells show appreciable degradation on being subjected to accelerated stress testing, type B cells show very little degradation, and type C and E cells lie between these extremes. While these conclusions demonstrate the applicability and potential usefulness of the technique, they should not be interpreted at this time as a quantitative measure of field degradation rates. It is felt that the technique is capable of such prediction, but considerable additional stress testing and analysis of laboratory and field degradation will be required before conclusive evidence can be demonstrated.

RELATIVE STRESS TEST EFFECTIVENESS

STRESS TEST	CELL TYPE			
	A	B	C	E
B-T	Dark	White	Diagonal	Diagonal
PRESSURE COOKER	Dark	Diagonal	Dark	Dark
85°C/85% R.H.	Diagonal	White	Diagonal	White
POWER CYCLE	White	White	White	White
THERMAL CYCLE	Dark	White	Diagonal	Diagonal
THERMAL SHOCK	Dark	White	Diagonal	Dark

Figure 13. Relative Effects of Accelerated Stress Tests on P_m .

RELATIVE STRESS TEST EFFECTIVENESS

STRESS TEST	CELL TYPE			
	A	B	C	E
B-T	Dark	Diagonal	Dark	Diagonal
PRESSURE COOKER	Dark	White	Dark	White
85°C/85% R.H.	Diagonal	White	White	White
POWER CYCLE	White	White	White	White
THERMAL CYCLE	Dark	Dark	Diagonal	Dark
THERMAL SHOCK	Dark	Dark	Diagonal	Dark

Figure 14. Relative Effects of Accelerated Stress Tests on Contact Integrity.

From an examination of the rows in Figures 13 and 14 it can be seen that the various tests vary in their effectiveness. The power cycle and 85°C/85% R.H. tests show little effect regardless of the cell type and for this reason may be omitted from future test schedules. Pressure cooker and thermal cycle tests show consistent degradation effects in most cell types, while BT testing strongly affects only one type of construction.

Because solar cells are so large (larger than any other semiconductor device) they could be expected to have thermal expansion problems as indicated by Figures 13 and 14. However, quantification of these problems is more difficult than in other tests. Cells which visually appear to have "catastrophically" failed by cracking may continue to show nominal power output, yet in reality must be considered incipient failures. Cracks can be detected, but before consistent power degradation occurs a second stress, such as BTH or vibration, must be applied.

With one exception, the observed P_m degradation could be directly related to failure of the cell metalization system, i.e., no unexplainable second order effects were observed. That one exception was the dissolution of the antireflective coating from the C cells under pressure cooker conditions. Thus the initial reasoning behind the design of the tests was vindicated.

Acknowledgements

The authors acknowledge the contributions of the following Clemson University research workers in the conduct of this program: Dr. L. T. Fitch, Dr. J. N. Thurston, Mr. K. Labib, Mr. C. Saylor, Mr. T. B. DuBose, Mr. R. C. Eng, Mr. D. Hawkins, Ms. D. Eggers, and Mr. D. Martins, all of the Department of Electrical and Computer Engineering. Special acknowledgement is made of the contributions of Mr. R. A. Hartman, Department of Electrical and Computer Engineering.